Mon. Not. R. Astron. Soc. **000**, 1–?? (2015) Printed 7 March 2016 (MN LATEX style file v2.2)

Galactic survey of ^{44}Ti sources with the IBIS telescope onboard *INTEGRAL*

Sergey S. Tsygankov,[1,2⋆] Roman A. Krivonos,[2] Alexander A. Lutovinov,[2,3] Mikhail G. Revnivtsev,[2] Eugene M. Churazov,[4,2] Rashid A. Sunyaev[4,2] and Sergey A. Grebenev[2]

[1] *Tuorla Observatory, Department of Physics and Astronomy, University of Turku, Väisäläntie 20, FI-21500 Piikkiö, Finland*
[2] *Space Research Institute of the Russian Academy of Sciences, Profsoyuznaya Str. 84/32, Moscow 117997, Russia*
[3] *Moscow Institute of Physics and Technology, Moscow region, Dolgoprudnyi, Russia*
[4] *Max Planck Institute for Astrophysics, Karl-Schwarzschild Str. 1, Garching, 85741, Germany*

arXiv:1603.01264v1 [astro-ph.HE] 3 Mar 2016

Accepted 2016 March 3. Received 2016 March 3; in original form 2015 December 11

ABSTRACT

We report the results of the deepest Galactic Plane ($|b| < 17.5°$) survey in the 67.9 and 78.4 keV nuclear de-excitation lines of titanium-44 (^{44}Ti) performed using the data acquired with the IBIS/ISGRI instrument onboard the *INTEGRAL* satellite during 12 years of operation. The peak sensitivity of our survey reached an unprecedented level of 4.8×10^{-6} ph cm^{-2} s^{-1} (3σ) that improves the sensitivity of the survey done by *CGRO*/COMPTEL by a factor of ~ 5. As a result, constraining upper limits for all sources from the catalog of Galactic supernova remnants (SNRs; Green 2014) are derived. These upper limits can be used to estimate the exposure needed to detect ^{44}Ti emission from any known SNR using existing and prospective X- and gamma-ray telescopes. Among the youngest Galactic SNRs, only Cas A shows significant ^{44}Ti emission flux in good agreement with the *NuSTAR* measurements. We did not detect any other sources of titanium emission in the Galactic Plane at significance level higher than 5σ confirming previous claims of the rarity of such ^{44}Ti-producing SNRs.

Key words: gamma-rays: ISM; supernova remnants; nuclear reactions, nucleosynthesis, abundances

1 INTRODUCTION

Supernova (SN) explosions determine the chemical and physical evolution of the Universe. An understanding of their mechanism is the keystone of many branches of the modern astrophysics. However, there is no way to observe directly physical processes during the first stages of the explosion due to a very high opacity. The most promising solution of this problem is to measure the amount of radioactive elements synthesised during SN explosion and based on that to verify the existing models (see, e.g., Vink 2012).

Probably the best candidate to such explosion tracer is radioactive isotope of titanium-44 (^{44}Ti). It has a lifetime of about 85 years (e.g., Ahmad et al. 2006), that is long enough to guarantee the substantial fraction of the synthesised titanium to remain active after the envelope become transparent. Such lifetime is much shorter than for, e.g., ^{26}Al ($\tau \sim 10^6$ yr), that permits to associate the measured flux with a specific supernova remnant (SNR), thus increasing chances to detect young (few hundred years) SNR.

^{44}Ti is produced during SN explosions deep inside the progenitor star and its yield is very sensitive to the particular conditions there. Mainly it is synthesised during core collapse SN within an α-rich freeze-out, and, hence, depends strongly on the expansion speed of the inner layers of the ejecta (Arnett 1996; Magkotsios et al. 2010). Other factors affecting yield of ^{44}Ti are the mass cut between the proto-neutron star and the ejecta, progenitor mass and metallicity, explosion asymmetry (Nagataki et al. 1998). Core collapse SNe produce typically 10^{-5}–10^{-4} M$_\odot$ of titanium (e.g. Timmes et al. 1996). The expected yield of ^{44}Ti in type Ia SNe is ranging from $\sim 10^{-6}$ M$_\odot$ for a centrally ignited pure-deflagration to $\sim 6 \times 10^{-5}$ M$_\odot$ for an off-center delayed detonation (Iwamoto et al. 1999; Maeda et al. 2010). However, in the so-called double-detonation sub-Chandrasekhar model it can reach $\sim 10^{-3}$ M$_\odot$ (Fink et al. 2010).

From the observational point of view the signatures of titanium decay through the chain ^{44}Ti→^{44}Sc→^{44}Ca can be observed in broad range of energies – it produces on average

⋆ E-mail:stsygankov@gmail.com

∼0.17, ∼0.88, ∼0.95 and ∼1 photons per one decay in the lines at energies 4.1, 67.9, 78.4, and 1157 keV, respectively. Hence, it could be detected by telescopes based on completely different principals (an overview of previous results is presented in Section 3.3).

Based on the comparison of the survey done by COMPTEL telescope onboard *Compton Gamma-Ray Observatory (CGRO)* in the 1.157 MeV line (Dupraz et al. 1997; Iyudin et al. 1999) with theoretical expectations The et al. (2006) concluded that SNe producing ^{44}Ti are not typical events. Particularly, they expect 5-6 positive detections of ^{44}Ti sources above COMPTEL's sensitivity limit ($\sim 10^{-5}$ ph cm^{-2} s^{-1} at 1σ level). However at that moment Cas A was the only confidently detected source of ^{44}Ti emission (Iyudin et al. 1994). It is worth noting that more recent calculations performed by Dufour & Kaspi (2013) give results consistent with one detected ^{44}Ti source in the survey with sensitivity reached by COMPTEL. Only recently, thanks to significant exposures collected by hard X-ray space telescopes currently operating in orbit (*INTEGRAL*/IBIS, *Swift*/BAT, *NuSTAR*), new evidence of SNRs emitting in ^{44}Ti lines started to appear, in particular SN 1987A (Grebenev et al. 2012; Boggs et al. 2015) and Tycho's SNR (Troja et al. 2014).

One of the main goal of the current paper is to search for new and previously unknown ^{44}Ti emission sources, serendipitous detections of which could provide us information about SN activity in the Milky Way within the last few centuries. Last systematic survey for ^{44}Ti sources in MeV domain was conducted by COMPTEL in the work of Dupraz et al. (1997) and Iyudin et al. (1999). The authors did not detect new unknown ^{44}Ti sources that was in agreement with canonical values of 2.5 to 3 Galactic SN events per century. Later, Renaud et al. (2004) confirmed the absence of new sources of ^{44}Ti line emission in the first survey of the Galactic Centre region ($|l| < 30^\circ$) using the *INTEGRAL* IBIS/ISGRI data from the first year of operation.

Core-collapse SNe can be embedded in the dense molecular clouds that gave birth to their massive progenitors. The high column densities of the Galactic, local molecular cloud, and even circumstellar obscuration may prevent detection of such a recent SN events. Undetectable at optical wavelength, young SNRs could be revealed through the decay of ^{44}Ti in emission lines at 67.9 and 78.4 keV thanks to high penetrating power of hard X-rays. As shown by recent detection of ^{44}Ti from SN 1987A in the Large Magellanic Cloud (LMC) by Grebenev et al. (2012), *INTEGRAL* IBIS/ISGRI has the potential for detecting these sources even in the nearby galaxies.

With sensitivity achieved in the current 12 years survey by *INTEGRAL*/IBIS in the Galactic Plane (factor of 2–5 better than COMPTEL) we can improve our knowledge about recent SN activity in the Galaxy by model independent and systematic-free imaging at better angular resolution ($12'$) in comparison to the COMPTEL experiment ($\sim 1^\circ$), which is, however still not enough to resolve spatial morphology of SNRs with typical size of a few arcmins.

In this paper we utilize main advantages of the *INTEGRAL*/IBIS telescope (large field of view, high sensitivity and energy resolution, huge amount of collected data) to systematically search for ^{44}Ti emission (in the two low-energy lines at 67.9 and 78.4 keV) from the Galactic SNRs, selected at $|b| < 17.5^\circ$.

2 OBSERVATIONS AND DATA ANALYSIS

The *INTEGRAL* observatory (Winkler et al. 2003) has demonstrated a great success in surveying the sky in hard X-rays at energies above 20 keV. Large field of view of $28^\circ \times 28^\circ$, moderate angular resolution of a few arcmins, and one of the highest sensitivity for the class of its optical design (coding aperture) led to many relevant survey papers (see, e.g., Krivonos et al. 2012 and references therein). Thanks to effective work of the IBIS coded-mask telescope (Ubertini et al. 2003) over more than ten years, we can conduct the first imaging survey of the whole Galactic Plane in titanium emission lines, significantly extending the work by Renaud et al. (2004) in the Galactic Centre. The fact that *INTEGRAL* spent most of its observational time towards the Galactic Plane, where most of the SNRs reside, makes the current survey unprecedented in sensitivity and coverage.

For the current analysis we utilized all the publicly available data taken until October, 2014 (or spacecraft revolution 1469). The data were screened and reduced in accordance with our previous surveys (see e.g. Churazov et al. 2005, 2014; Krivonos et al. 2010 and references therein). To take into account the long-term ISGRI detector degradation and subsequent decrease in the efficiency (Caballero et al. 2013) we corrected for a secular gain variations and adjusted the efficiency in each IBIS/ISGRI energy bands using the flux of the Crab nebula measured in the observation that is closest in time (for details see Krivonos et al. 2012). This method corresponds to a smooth recalibration of the ancillary response function (ARF) over the time span of the survey. In our IBIS/ISGRI data analysis we use the diagonal energy redistribution matrix designed to reproduce Crab spectrum in the form

$$\mathrm{d}N/\mathrm{d}E = 10.0 \times E_{\mathrm{keV}}^{-2.1} \text{ phot cm}^{-2} \text{ s}^{-1} \text{ keV}^{-1} \quad (1)$$

which is a good representation of the historic Crab observations (see, e.g., Churazov et al. 2007).

The total list of the available data over the full sky contains 99108 individual *INTEGRAL* pointings with typical exposure of 2 ks, or so called *Science Window*s (*ScW*s), which corresponds to ∼ 178 Ms of the effective exposure. The data of the ISGRI detector layer (Lebrun et al. 2003) for each ScW were converted into sky images in the energy bands of interest (defined below). Similar to the *INTEGRAL* nine-year Galactic Plane survey by Krivonos et al. (2012), the survey mosaicing was organized in six overlapping $70^\circ \times 35^\circ$ Galactic cartesian map projections centered at $b = 0^\circ$ and $l = 0^\circ$ (GC), $\pm 50^\circ$, $\pm 115^\circ$, and $l = 180^\circ$ (Galactic anticenter). The latitude coverage of the current survey $|b| < 17.5^\circ$ was chosen to take advantage of the large IBIS field of view and *INTEGRAL* observational pattern in the Galactic Plane. The final data set used in this work comprises 62509 *ScW*s or 104 Ms of dead-time corrected exposure, which corresponds to about 60% of the full data set.

The search for the ^{44}Ti lines at 67.9 and 78.4 keV imposes severe requirements on energy calibration precision of

Table 1. Working energy bands for the current ^{44}Ti survey.

Name	Range [keV]	Width [keV]	1 mCrab [erg s^{-1} cm^{-2}] [ph cm^{-2} s^{-1}]	^{44}Ti lines
E1	25.0 – 40.0	15.0	5.35×10^{-12}	
			1.07×10^{-4}	
E2	40.0 – 64.6	24.6	5.19×10^{-12}	
			6.45×10^{-5}	
E3	64.6 – 71.2	6.6	1.02×10^{-12}	67.9 keV
			9.48×10^{-6}	67.9 keV
E4	71.2 – 74.6	3.4	0.48×10^{-12}	
			4.14×10^{-6}	
E5	74.6 – 82.2	7.6	1.00×10^{-12}	78.4 keV
			8.01×10^{-6}	78.4 keV
E6	82.2 – 130.0	47.8	4.65×10^{-12}	
			2.84×10^{-5}	
E7	64.6 – 82.2	17.6	2.52×10^{-12}	both
			2.17×10^{-5}	both

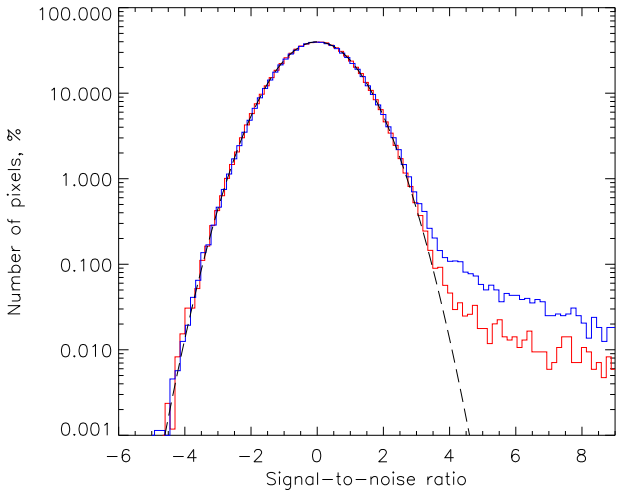

Figure 1. Distribution of signal-to-noise ratio values of a number of pixels in 70° × 35° sky map centered at $l = 0°$ (blue line) and $l = +50°$ (red line) in E7 energy band (see Table 1). The long-dashed line represents normal distribution with zero mean and unit variance.

the instruments. We used the most up-to-date ISGRI energy reconstruction available through the Offline Scientific Analysis (OSA) version 10.1, provided by ISDC[1]. As described by Caballero et al. (2013), the energy resolution of ISGRI at tungsten (W) fluorescent line located at 58.8297 keV shows gradual broadening from ∼ 5 to ∼ 10 keV (FWHM) over 10 years of the current mission life span, which still makes it possible to study narrow ^{44}Ti emission lines. To trace continuum and line emission we defined working energy bands as shown in Table 1. Two ^{44}Ti lines at 67.9 and 78.4 keV are accommodated in the energy bands E3 and E5, respectively, and both lines are placed in E7 band. E5 is wider than E3 by 1 keV owing to an initial ISGRI energy resolution of 8% at 60 keV (Lebrun et al. 2003). According to our measurements, the average energy resolution (FWHM) at 60 keV over the survey data span is ∼ 7.5 keV, which is comparable to the width of the selected energy bands and consistent with Caballero et al. (2013). To prevent any losses in the ^{44}Ti line emission due to the finite energy resolution as a reference energy band we took much broader E7 band containing both lines.

Despite the great improvement of the ISGRI detector absolute energy reconstruction in OSA 10.1 compared to previous versions, the ∼ 1.5% gain variations during each orbit are still present, which lead to ∼ 1 keV uncertainty at ∼ 80 keV. We applied additional gain correction based on the position of the tungsten fluorescent line, suppressing the uncertainty of energy reconstruction for the detector-averaged line centroid to less than 0.1 keV.

Table 1 contains flux conversion coefficients between different flux units (mCrab and erg s^{-1} cm^{-2}, and ph cm^{-2} s^{-1}) in our working energy bands assuming Crab spectrum in the form given by eq. (1).

[1] ISDC Data Centre for Astrophysics, http://www.isdc.unige.ch/

3 RESULTS

3.1 The search for new sources of ^{44}Ti line emission

The search for new sources has been performed on each projected mosaic images in the reference energy band E7 (64.6 – 82.2 keV) containing both ^{44}Ti lines and therefore providing better statistics. We defined detection threshold allowing not more than one false detection assuming pure photon counting statistics. Given the angular resolution of the IBIS telescope (12′), the Galactic survey ($|b| < 17.5°$) contains ∼ 3×10^5 independent pixels which can generate one statistical fluctuation at 4.7σ. We should stress that the sensitivity of our ^{44}Ti survey is limited by count statistics only and not affected by systematics, which seriously limits the sensitivity of IBIS telescope at lower energies, especially in the crowded region of the Galactic Centre (see, e.g., Krivonos et al. 2010b, 2012). Fig. 1 shows a signal-to-noise distribution of pixel values in the sky mosaic at $l = 0°$ (blue line) and $l = +50°$ (red line) along with the normal distribution representing a statistical noise. Note that the positive tail of this distribution is formed by continuum sources. As seen from the figure (overall shape and, in particular, negative side of the distribution), the observed noise distribution can be very well described by normal distribution with zero mean and unit variance.

The source detection sensitivity of our ^{44}Ti survey is not completely uniform over the Galactic Plane (Fig. 2). The maximum IBIS/ISGRI sensitivity is achieved in the region of the Galactic Center (GC) which exhibit the largest exposure accumulated over 12 years. The survey sky coverage in 64.6–82.2 keV energy band (E7) as a function of a 4.7σ limiting flux is demonstrated in Fig. 3. The peak sensitivity is about 0.7 mCrab (1.8×10^{-11} erg s^{-1} cm^{-2} in E7 band) in the GC. Regarding the range of the Galactic latitudes $|b| < 17.5°$, the survey covers 10% of its geometrical area (12680 deg^2) at

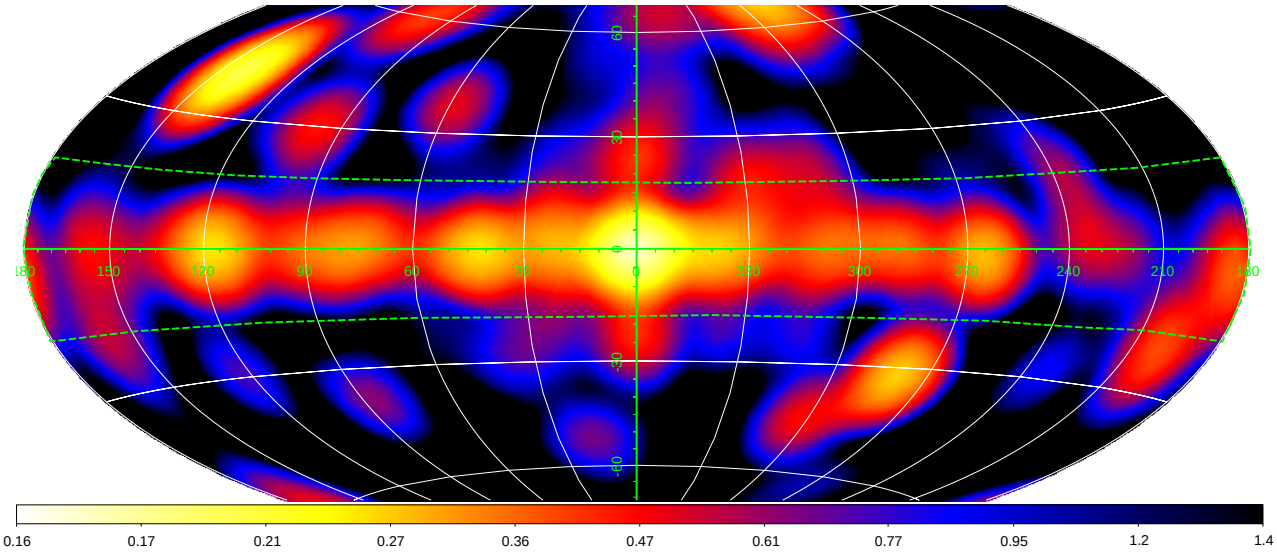

Figure 2. The map shows 1σ flux sensitivity in 64.6–82.2 keV energy band (E7; Table 1) ranging from 0.16 to 1.4 mCrab. Two dashed green lines comprise geometrical area of the survey ($|b| < 17.5°$).

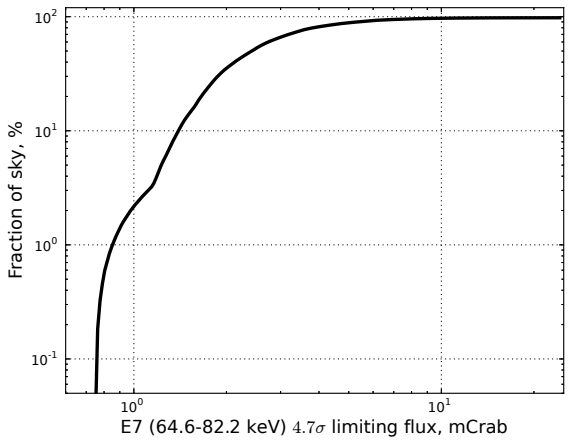

Figure 3. Fraction of the sky covered as a function of 4.7σ limited flux. 100% corresponds to geometrical area of the survey (12680 deg^2).

1.4 mCrab (3.5×10^{-11} erg s^{-1} cm^{-2}) and 90% at 5.4 mCrab (1.4×10^{-10} erg s^{-1} cm^{-2}).

The peak sensitivity of our survey reached in the region of the Galactic centre is 1.0×10^{-5} ph cm^{-2} s^{-1} (3σ) in E7 energy band, containing both 67.9 keV and 78.4 keV lines. Taking into account the approximate equality of intensities in these two lines the 3σ sensitivity per one ^{44}Ti line in the current *INTEGRAL*/IBIS survey can be recalculated as $\sim 4.8\times10^{-6}$ ph cm^{-2} s^{-1}. According to the different efficiencies of emission in different lines the corresponding sensitivity in the 1.157 MeV line is $\sim 5.2\times10^{-6}$ ph cm^{-2} s^{-1}. This is factor of ~ 5 better than sensitivity of 2.7×10^{-5} ph cm^{-2} s^{-1} in the 1.157 MeV line (3σ) reached with the COMPTEL experiment in the Galactic Plane (Dupraz et al. 1997; Iyudin et al. 1999). Regarding the Galactic Plane at $|l| < 50°$ a factor of ~ 2 improvement in sensitivity is achieved. To illustrate the improvement of sensitivity in the current survey in comparison to the COMPTEL one, we constructed the age-distance diagram assuming a ^{44}Ti yield of $Y_{44} = 1\times10^{-4}$ M$_\odot$ (see Fig. 4; ages and distances for the plotted SNRs are listed in Table 3).

The list of candidate sources detected with $S/N > 4.7\sigma$ and within latitude range of the current survey ($|b| < 17.5°$) contains only one previously unknown object, the source IGR J18406+0451 found at position R.A.=18h 40m 40.80s, Decl.=04d 51m 36.0s (equinox J2000), which is $15'$ away from the known low mass X-ray binary Serpens X-1 (Liu et al. 2007, listed as 3A 1837+049). The source was registered with a flux of 1.4 ± 0.28 mCrab (5.0σ detection) in the E7 energy band. The localization accuracy of the sources detected with IBIS/ISGRI depends on the source significance (Gros et al. 2003; Bird et al. 2006). According to Krivonos et al. (2007), the positional 1σ uncertainty of the source detected at $S/N \simeq 5-6\sigma$ is $2.1'$.

To further investigate the properties of IGR J18406+0451 we reconstructed its flux in all energy bands E1-E7. IGR J18406+0451 does not show significant detection in E1 ($<$ 0.23 mCrab, 3σ); in E2 ($<$ 0.35 mCrab, 3σ); and in E6 ($<$ 0.84 mCrab, 3σ) but exhibits marginal detection in E3 (1.09 ± 0.39 mCrab, 2.8σ); E4 (1.51 ± 0.69 mCrab, 2.19σ), and E5 (1.63 ± 0.51 mCrab, 3.2σ).

Assuming IGR J18406+0451 is a ^{44}Ti emission source, the combined probability of ^{44}Ti line detection in E3 and E5 is 7×10^{-6} ($\sim 4.5\sigma$), which is lower than the E7 significance (5.0σ). This tells us that intermediate energy band E4 can contain some contribution from ^{44}Ti lines probably due to the ISGRI spectral resolution (5–10 keV) at these energies. This assumption is confirmed by the combined probability of signal detection in E3/E4/E5 bands, which is 7×10^{-6} or 5.2σ.

In all energy bands of the continuum emission E1, E2 and E6, IGR J18406+0451 is below the detection threshold, while the source shows significant ($\sim 5\sigma$) emission in E7

energy band containing two ^{44}Ti emission lines, and this excess is dominated by the flux in E3 and E5 bands, where the two low-energy ^{44}Ti lines are located. Owing to a relatively high Galactic latitude of 4.6°, we can expect the source candidate IGR J18406+0451 to be nearby, in particular if it is the remnant of a core-collapse SN, potentially located in the Sagittarius spiral arm at 2–3 kpc (Zhang et al. 2009).

In spite of a relatively high S/N ratio for this new source it is still not far from the detection threshold (4.7σ) corresponding to the registration of one false source in our survey. Therefore additional observational evidence are required to establish if the source is real or not.

For this purpose, we asked for DDT observations of this region with the *XMM-Newton* observatory. These observations were performed on October 9, 2015 with a total exposure of ~ 30 ksec. Data were reduced with the standard SAS software[2]. No bright sources were detected inside the *INTEGRAL* error circle. The search for faint sources met some difficulties due to the illumination from the bright nearby source Serpens X-1. A conservative point-source upper limit (3σ) on the flux at the IGR J18406+0451 position is about 8×10^{-14} ph cm^{-2} s^{-1} in the 0.5-10 keV energy band (under the assumption of a power-law spectrum with slope $\Gamma = -2$).

It is important to note, that apart from hard X-ray emission lines at 67.9 and 78.4 keV, there is another one originated from the ^{44}Ti decay – the ^{44}Sc fluorescence line with the ^{44}Ti emission in this line (with a branching ratio of 0.17 per decay). The averaged nuclear de-excitation lines flux measured from IGR J18406+0451 $F_{44} = 1.27 \times 10^{-5}$ ph cm^{-2} s^{-1} can be translated into the expected flux in the 4.1 keV line $F_{4.1keV} = 2.16 \times 10^{-6}$ ph cm^{-2} s^{-1}. An upper limit (3σ) for the flux in the narrow energy band 3.9-4.3 keV, derived from the *XMM-Newton* data, is $\simeq 8 \times 10^{-7}$ ph cm^{-2} s^{-1}, that is several times lower than the above estimations. Note that the expected flux in the 4.1 keV line is true for the fully transparent SNR envelope and with no additional absorption by the ISM gas along the line of sight at these soft X-ray energies.

The obtained results can be interpreted in two ways: the source candidate IGR J18406+0451 is a false detection or its emission in soft X-rays is strongly absorbed. Thus, additional observations in hard X-rays by instruments with a better sensitivity and angular resolution (like *NuSTAR*) are required to confirm the detection of IGR J18406+0451.

3.2 A catalogue of Galactic supernova remnants

Thanks to the wide field of view and good angular resolution of the IBIS telescope we can for the first time put upper limits on the ^{44}Ti line emission from all known Galactic SNRs. For this purpose we used the catalog of Galactic SNRs presented in Green (2014). The catalogue contains 294 sources revealed through radio and infra-red surveys, as well as X-ray observations. Most of the SNRs are old, and generally we do not expect to detect significant signal from them, but no systematic search for ^{44}Ti emission has been performed so far. Since we are looking at known sky positions, we can go below detection threshold of the current survey (4.7σ) and provide marginal detection or conservative upper limit.

[2] `http://xmm2.esac.esa.int/sas/`

Table 2 lists measured fluxes or 3σ upper limits towards 294 SNRs from Green (2014). As indicated in the notes to the table, 60 SNRs are subject to spatial confusion within $12'$ (the IBIS/ISGRI angular resolution) from known hard X-ray sources. The measured flux of 9 SNRs is most probably dominated by the continuum emission of the associated X-ray source, rather than by putative ^{44}Ti line emission. If significance of the detection of such source is above 3σ level, an upper limit (3σ) in the 78.4 keV line is also shown assuming a simple power-law continuum model. Marginal detection (at less than 3σ) of the ^{44}Ti line emission and/or continuum is registered from Tycho SNR (see Sec.3.3), G065.7+01.2, G069.0+02.7, G315.1+02.7 and G356.3–01.5.

3.3 Historical supernovae and other reported sources of ^{44}Ti

One of the main goals of this survey was to verify the ^{44}Ti line fluxes from historical SNRs reported in the literature and to provide an independent estimate of the corresponding amount of synthesised ^{44}Ti with much larger statistics available thanks to the whole *INTEGRAL* IBIS/ISGRI dataset. List of the young (with ages not more than ~ 1000 years) Galactic SNRs with known (or estimated) dates of explosion and distances used in our study is presented in Table 3.

To estimate the ^{44}Ti flux in the most robust way we used the simplest model for the continuum emission – power-law. This model is usually assumed for fitting the continuum of SNRs in the hard X-ray domain although it is known that synchrotron emission does exhibit spectral steepening beyond the cutoff energy (e.g. Reynolds 1998; Zirakashvili & Aharonian 2007). To take into account ^{44}Ti emission lines we introduced to the model two Gaussians with fixed positions at 67.9 and 78.4 keV, and intrinsic widths fixed at 10^{-3} keV. Additionally fluxes in the two lines were tied as $F_{68} = 0.93F_{78}$. For the fitting procedure we used XSPEC v.12.8.1g.

Cassiopeia A

First detection of ^{44}Ti line emission from Cas A has been reported by CGRO/COMPTEL (Iyudin et al. 1994), with a flux of $(3.4 \pm 0.9) \times 10^{-5}$ph cm^{-2} s^{-1}(Schönfelder et al. 2000). Later, this finding was confirmed by *BeppoSAX* observations which resulted in detection of the 67.9 and 78.4 keV lines (Vink et al. 2001). The line flux was dependent on the continuum shape, being $(1.9 \pm 0.4) \times 10^{-5}$ph cm^{-2} s^{-1}assuming a simple power-law spectrum.

Renaud et al. (2006a) using about 4.5 Ms of *INTEGRAL*/ISGRI total exposure time detected both 67.9 and 78.4 keV lines with a flux of $(2.5 \pm 0.3) \times 10^{-5}$ph cm^{-2} s^{-1}that corresponds to a synthesised ^{44}Ti mass of $1.6^{+0.6}_{-0.3} \times 10^{-4}$ M$_\odot$. In a more recent work by Siegert et al. (2015) the *INTEGRAL*/SPI data were utilized. Measured fluxes in the 78.4 keV and 1157 keV lines are $(2.1 \pm 0.4) \times 10^{-5}$ph cm^{-2} s^{-1}and $(3.5 \pm 1.2) \times 10^{-5}$ph cm^{-2} s^{-1}, which corresponds to $(1.5 \pm 0.4) \times 10^{-4}$ and $(2.4 \pm 0.9) \times 10^{-4}$ M$_\odot$ of ^{44}Ti, respectively. Authors also pointed out that the reason for a significantly larger flux in the 1157 keV line possibly could be an additional contribution to this line from nuclear de-excitation following energetic particle collisions in the remnant and swept-up material.

Table 2. A sample of the catalogue of Galactic SNRs (Green 2014) with measured fluxes or 3σ upper limits in the $64.6-82.2$ keV band. The full version is available in the online version of this article.

No.	Name[1]	l^{II} deg	b^{II} deg	$\mathrm{Flux}_{64.6-82.2\ \mathrm{keV}}$,[2] 10^{-12} erg cm^{-2} s^{-1}	Notes[3]
001	SNR G000.0+00.0	-0.042	-0.054	N/A	confusion (AX J1745.6-2901)
< ... >					
144	SNR G094.0+01.0	93.974	1.026	< 2.64	
145	SNR G096.0+02.0	96.043	1.953	< 2.79	
146	SNR G106.3+02.7	106.273	2.705	< 2.54	
147	SNR G108.2−00.6	108.193	-0.627	< 2.27	
148	SNR G109.1−01.0	109.142	-1.015	2.63 ± 0.73 (3.60)	continuum (2E 2259.0+5836); $F_{78} < 1 \times 10^{-5}$ ph cm^{-2} s^{-1}
149	SNR G111.7−02.1	111.734	-2.145	7.31 ± 0.68 (10.75)	Cas A
150	SNR G113.0+00.2	114.088	-0.213	< 1.89	
< ... >					
294	SNR G359.1−00.5	-0.879	-0.506	< 1.17	confusion (IGR J17446-2947)

[1] Catalogue is sorted by source name, which is in turn, based on Galactic coordinates.
[2] The upper limits are given at 3σ confidence level. In case of a source detection, the significance is shown in parenthesis.
[3] The spatial confusion with a known hard X-ray source (shown in parenthesis) is indicated. SNRs dominated by the continuum flux are marked as well. If significance of the detection of such source is above 3σ level, an upper limit (3σ) in the 78.4 keV line is shown assuming a simple power-law continuum model.

Table 3. List of the young (with ages not more than ~ 1000 years) Galactic SNRs with known (or estimated) dates of explosion and distances.

Name	l	b	Exposure, Ms[1]	SNR age, years	Distance, kpc	Type	References[2]
G1.9+0.3	1.871	0.326	18.1	110 ± 11	8.5	Ia	1, 2
Kepler	4.526	6.820	11.2	410	$3.9^{+1.4}_{-0.9}$	Ia	3, 4
G21.5−0.9	21.501	−0.885	5.1	870^{+200}_{-150}	4.7 ± 0.4	II	5, 6
Kes 75	29.702	−0.248	4.8	~ 730	6.3 ± 1.2	II	7, 8
Cas A	111.734	−2.145	5.9	343	$3.4^{+0.3}_{-0.1}$	IIb	9, 10, 11
Tycho	120.087	1.423	6.8	442	4 ± 1	Ia	12, 13
SN 1181	130.718	3.084	2.7	833	2.0 ± 0.3	II	14
Crab	184.557	−5.784	3.8	960	2.0 ± 0.5	II	15
G310.6−1.6	310.592	−1.593	3.3	~ 1000	7 ± 2	II	16
SN 1006	327.572	14.566	2.5	1008	2.18 ± 0.08	Ia	17

[1] Dead-time corrected effective exposure of the *INTEGRAL*/IBIS telescope
[2] References: (1) Reynolds et al. (2008), (2) Carlton et al. (2011), (3) Sankrit et al. (2005), (4) Reynolds et al. (2007), (5) Bietenholz & Bartel (2008), (6) Camilo et al. (2006), (7) Gotthelf et al. (2000), (8) Leahy & Tian (2008), (9) Thorstensen, Fesen, & van den Bergh (2001), (10) Reed et al. (1995), (11) Krause et al. (2008a), (12) Hayato et al. (2010), (13) Krause et al. (2008b), (14) Kothes (2013), (15) Trimble (1973), (16) Renaud et al. (2010), (17) Winkler, Gupta, & Long (2003).

Using the high spatial resolution and sensitivity of the *NuSTAR* focusing high-energy X-ray telescope, Grefenstette et al. (2014) were able to map the distribution of ^{44}Ti emission over the Cas A supernova remnant. Their result confirmed previous claims of a highly asymmetric explosion, needed to explain the observed amount of synthesised ^{44}Ti. Spectroscopic studies also revealed a redshift of the 67.9 keV line by 0.47 ± 0.21 keV, with a flux of $(1.5 \pm 0.3) \times 10^{-5}$ph cm^{-2} s^{-1}.

Our analysis confirmed the presence of a highly significant emission component in the E7 energy band above the continuum described by a simple power-law model with photon index of 2.9 ± 0.1. The obtained flux in the 67.9 keV line is $F_{68} = (1.3 \pm 0.3) \times 10^{-5}$ ph cm^{-2} s^{-1}. Both continuum and line parameters are compatible within $1-2\sigma$ with results from Renaud et al. (2006a) based on smaller sample of IBIS/ISGRI data. Also this values agree very well with the recent *NuSTAR* result and most of previously published measurements.

G1.9+0.3

One of the most promising sources of ^{44}Ti emission in our sample is G1.9+0.3. Based on the detected expansion between 1985 and 2007 Reynolds et al. (2008) estimated its age around 100 years, making this SNR the youngest one in the Galaxy at distance around 8.5 kpc from the Sun. Using the *Chandra* observations Borkowski et al. (2010) detected a 4.1 keV line which was attributed to ^{44}Sc fluorescence emission. The estimated mass of synthesised ^{44}Ti is (1–7) $\times 10^{-5}$ $M_\odot$ that corresponds to an expected flux in the 67.9 and 78.4 keV nuclear de-excitation lines around (0.3–2.3) $\times 10^{-5}$ph cm^{-2} s^{-1}. Later, the *NuSTAR* observa-

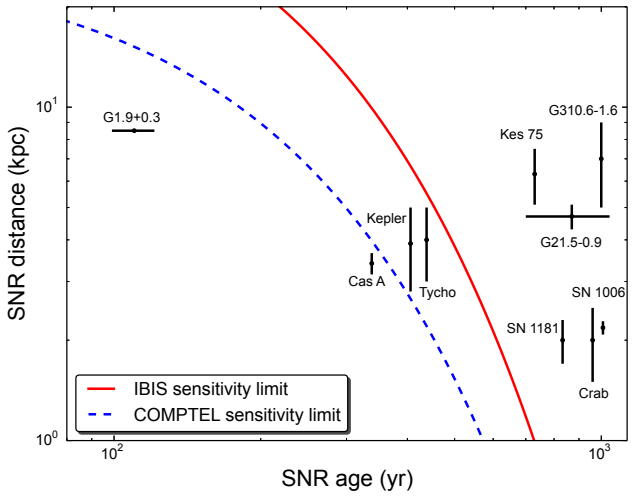

Figure 4. Age-distance diagram showing the capability of ^{44}Ti emission detection using the COMPTEL and current Galactic *INTEGRAL*/IBIS surveys. The red solid line and blue dashed line show 1σ peak sensitivity reached in the current *INTEGRAL*/IBIS survey ($\sim 1.7 \times 10^{-6}$ph cm^{-2} s^{-1}) and COMPTEL survey (9×10^{-6}ph cm^{-2} s^{-1}), correspondingly. A ^{44}Ti lifetime of 85.0 yr and a yield of 1×10^{-4} M$_\odot$ were assumed.

tory put a 95% upper limit for the 67.9 keV line around 1.5×10^{-5}ph cm^{-2} s^{-1}for an assumed line width (1 sigma) of 4 keV (Zoglauer et al. 2015).

In our survey we did not detect a significant flux from G1.9+0.3 with a corresponding 3σ upper limit of 9×10^{-6} ph cm^{-2} s^{-1}. This upper limit is more constraining than the one obtained with *NuSTAR* but still compatible within the errors with the reported 4.1 keV line flux.

GRO J0852-4642 / RX J0852.0-4622 / G266.2-1.2 / Vela Jr

COMPTEL discovered a source of ^{44}Ti line emission from a previously unknown Galactic SNR in the Vela region, named Vela Jr, with a flux of $(3.8 \pm 0.7) \times 10^{-5}$ph cm^{-2} s^{-1}in the 1.157 MeV line (Iyudin et al. 1998). Later Schönfelder et al. (2000) have shown this detection to be much less significant due to technical issues related to the background modeling and event selection. Doubts about the reality of the ^{44}Ti line detection were also raised by the age and distance estimates pointed towards a more distant and older SNR than originally thought (e.g. Slane et al. 2001; Katsuda, Tsunemi, & Mori 2008). At lower energies some evidence of 4.1 keV line identified with ^{44}Sc were reported by Tsunemi et al. (2000), Iyudin et al. (2005) and Bamba, Yamazaki, & Hiraga (2005). However, Slane et al. (2001) and Hiraga et al. (2009) did not confirm these detections, making future studies very important.

In our survey we did not detect the signal from the ^{44}Ti decay. The corresponding 3σ upper limit is 1.8×10^{-5} ph cm^{-2} s^{-1}. Thus the *INTEGRAL*/IBIS measurement excludes the detection made by the COMPTEL experiment under assumption of a point-like source, confirming results of similar analysis performed by Renaud et al. (2006b). Taking into account that SNR has a diameter of 2°, a more detailed study should be carried out in order to properly derive a consistent upper limit as a function of the source extent.

Tycho's Supernova / SN 1572

The *Swift*/BAT telescope discovered a significant emission excess above the continuum level in the 60–85 keV energy band in the spectrum of Tycho SNR (Troja et al. 2014). It is the first evidence for a detection of ^{44}Ti decay emission in a Type Ia SNR. The flux in the 78.4 keV line was measured to be $(1.4 \pm 0.6) \times 10^{-5}$ph cm^{-2} s^{-1}that corresponds to a ^{44}Ti mass around 10^{-4} M$_\odot$ depending on the distance to the SNR (see Troja et al. 2014). Marginal detection (significance level $\sim 2.6\sigma$) of a bump feature in the 60–90 keV band was reported also by Wang & Li (2014) using the *INTEGRAL*/IBIS telescope data. The corresponding 3σ upper limit for the ^{44}Ti line emission of 1.5×10^{-5}ph cm^{-2} s^{-1}which coincides with earlier result obtained by Renaud et al. (2006b) using the *INTEGRAL*/IBIS data as well. An indication of the spatial co-location of the post-shock Ti with other iron-peak nuclei was found using *XMM-Newton* data (Miceli et al. 2015).

However, the more recent *NuSTAR* observations did not find evidence for ^{44}Ti emission in the spectrum of Tycho SNR with the upper limit $F_{78} < 7.5 \times 10^{-6}$ ph cm^{-2} s^{-1} (90% confidence level), ruling out the above-mentioned *Swift*/BAT and *INTEGRAL*/IBIS detections (Lopez et al. 2015). The corresponding upper limit on the ^{44}Ti yield was found to be $M_{44} < 8.4 \times 10^{-5}$ M$_\odot$ assuming distance to the SNR of 2.3 kpc.

To shed further light on the existence of the ^{44}Ti emission in the spectrum of Tycho SNR we have performed a fit to the measured IBIS/ISGRI spectrum, as for the other young SNRs in our sample. With the achieved sensitivity we can not confidently confirm the detection made by *Swift*/BAT (Troja et al. 2014). Inclusion of the ^{44}Ti lines into the fitting model consisting of a simple power-law gives a flux in the 78.4 keV line $F_{78} = (5 \pm 3) \times 10^{-6}$ ph cm^{-2} s^{-1}, compatible with the above-mentioned upper limit obtained with *NuSTAR* (Lopez et al. 2015).

Kepler

Detection of the ^{44}Ti emission from the Kepler SNR has not been claimed so far. 3σ upper limit in 1.157 MeV line obtained in the COMPTEL Galactic survey is 1.8×10^{-5} ph cm^{-2} s^{-1} (Dupraz et al. 1997; Iyudin et al. 1999). We did not detect a significant flux from the source in any working energy bands (see Tab. 1) either. Upper limit obtained in our survey is 6.3×10^{-6} ph cm^{-2} s^{-1}(3σ) per line.

SN 1987A

The only known extragalactic source of ^{44}Ti decay emission is SN 1987A in the Large Magellanic Cloud where the *INTEGRAL*/IBIS telescope detected significant flux in the 67.9 and 78.4 keV lines (Grebenev et al. 2012). The combined flux in both lines was measured to be $(1.5 \pm 0.4) \times 10^{-5}$ph cm^{-2} s^{-1}that can be translated into a ^{44}Ti mass of $(3.1 \pm 0.8) \times 10^{-4}$ M$_\odot$. Later the *NuSTAR* telescope confirmed the existence of both lines, but with somewhat lower flux corresponding to a ^{44}Ti yield of $(1.5 \pm 0.3) \times 10^{-4}$ M$_\odot$ (Boggs et al. 2015).

The *INTEGRAL* survey described above includes additional data compared to Grebenev et al. (2012) and leads to a slightly smaller line flux of $\sim 1 \times 10^{-5}$ph cm^{-2} s^{-1}corresponding to ^{44}Ti mass of $\sim 2 \times 10^{-4}$

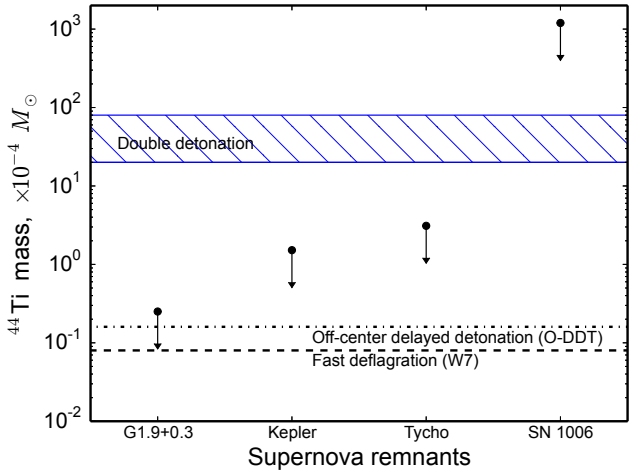

Figure 5. Arrows show 3σ upper limits on the ^{44}Ti yield for Type Ia historical SNe obtained in this work. Ages and distances for each SNR are taken from Table 3. The ^{44}Ti mass predictions from different explosion models are shown as well.

$M_\odot$ which is closer to the value obtained by *NuSTAR*. Because SN 1987A is located in another galaxy (LMC) a detailed analysis will be published in a separate paper (Grebenev et al., in preparation).

Per OB2

In addition to the aforementioned sources one can point another potential source of ^{44}Ti emission located in the region of Perseus OB2 association. Some hints of a weak signal (at significance level around $\sim 3\sigma$) in the 1.157 MeV line from this region was reported by Dupraz et al. (1997) using the COMPTEL data. We did not detect any significant point-like source in the vicinity of Per OB2 with 3σ upper limit ~ 1.5 mCrab (3.3×10^{-5} ph cm^{-2} s^{-1}).

4 SUMMARY

In this work we performed a systematic search for ^{44}Ti line emission at 67.9 and 78.7 keV with the IBIS/ISGRI instrument aboard the *INTEGRAL* observatory. The long exposure collected by the mission in the Galactic Plane allowed us to put strong limits on the ^{44}Ti line emission and improve the previous constraints made with COMPTEL experiment in the 1.157 MeV ^{44}Ti line emission by a factor of 2–5.

Sensitivity of the current survey is governed by photons count statistics only which allowed us to set up the lowest possible detection threshold while not flooding the catalog of candidate sources by false detections. Expecting only one statistical fluctuation above 4.7σ, we detected a ^{44}Ti source candidate IGR J18406+0451 with S/N=5σ. However, deep *XMM-Newton* observation does not show the presence of a bright source in this region, indicating that IGR J18406+0451 is either a false detection or its emission in soft X-rays is strongly absorbed (either locally or due to the ISM gas along the line of sight).

Among historical SNRs only Cas A shows significant detection with a flux $F_{68} = (1.3 \pm 0.3) \times 10^{-5}$ ph cm^{-2} s^{-1} in agreement with most of previously published measurements. This flux corresponds to $(1.1 \pm 0.3) \times 10^{-4}$ $M_\odot$ of ^{44}Ti that is at the upper boundary of the theoretical predictions for core-collapse SNe (see, e.g., Timmes et al. 1996).

We put strong upper limits on the detection of ^{44}Ti emission in other historical SNRs and potential ^{44}Ti sources mentioned in the literature: Vela Jr, Tycho (SN1572), Per OB2 and G1.9+0.3. Regarding the latter, we derived a more constraining upper limit on the ^{44}Ti line emission than that obtained with *NuSTAR* (Zoglauer et al. 2015) by a factor of few.

Predicted ^{44}Ti yield for Type Ia SNe is scattered from $\sim 8 \times 10^{-6}$ $M_\odot$ in the classical deflagration model (W7 in Nomoto, Thielemann, & Yokoi 1984; Maeda et al. 2010) to $few \times 10^{-3}$ $M_\odot$ in the so-called double detonation sub-Chandrasekhar model, when the explosion is triggered by an explosion at the surface of the white dwarf (models 1-4 in Fink et al. 2010).

Figure 5 shows the comparison of the 3σ upper limits on the ^{44}Ti yield from Type Ia SNe obtained in this work with predictions of different models. Such extreme models as double detonation (Fink et al. 2010) or helium deflagration (Woosley & Kasen 2011), predicting $> 10^{-3}$ $M_\odot$ of ^{44}Ti, are clearly ruled out by the observational data. At the same time broad range of models predicting ^{44}Ti yields below $\sim 10^{-5}$ $M_\odot$ is consistent with our results. For the illustration purposes in Fig. 5 the fast deflagration W7 model (Nomoto, Thielemann, & Yokoi 1984) and delayed detonation model which follows an extremely off-center deflagration (O-DDT model in Maeda et al. 2010) are shown by dashed and dash-dot lines, respectively.

Finally we put strong upper limits for all Galactic SNRs reported in the catalog by Green (2014). The obtained upper limits can be used to estimate the exposure times needed to detect ^{44}Ti emission from any known SNR using existing and prospective X- and gamma-ray telescopes. Moreover, more or less homogeneous coverage of the Galactic Plane with *INTEGRAL* (see Fig. 2) permits to estimate an upper limit on the titanium emission from any potentially interesting place in the Galaxy: starburst regions, high-absorption regions such as the spiral arm tangents, and to revisit the issue about the main sources of Galactic ^{44}Ca (The et al. 2006; Dufour & Kaspi 2013). In particular, well known giant molecular cloud Sagittarius B2 (Sgr B2) located about 120 pc from the center of the Milky Way emits not more than 5.1×10^{-6} ph cm^{-2} s^{-1} (3σ upper limit) per ^{44}Ti line; the Orion Molecular Cloud Complex containing many bright nebulae, dark clouds, and young stars has a 3σ upper limit of 1.5×10^{-5} ph cm^{-2} s^{-1}per line; a 3σ upper limit for the flux from the Norma and Sagittarius spiral arms tangents is 1.0×10^{-5} ph cm^{-2} s^{-1} per line. Among extragalactic objects one of the most interesting is the Tarantula Nebula (known as 30 Doradus) in the Large Magellanic Cloud. This most active starburst region in the Local Group emits less than 0.9×10^{-6} ph cm^{-2} s^{-1}.

ACKNOWLEDGMENTS

The work was supported by Russian Science Foundation (grant 14-22-00271). We thank the anonymous referee whose suggestions helped improve and clarify the manuscript. The

results of this work are based on observations of the INTEGRAL observatory, an ESA project with the participation of Denmark, France, Germany, Italy, Switzerland, Spain, the Czech Republic, Poland, Russia and the United States. Results are also partly based on observations obtained with XMM-Newton, an ESA science mission with instruments and contributions directly funded by ESA Member States and NASA. We are grateful to the XMM-Newton team for the acceptance and execution of our DDT request. Authors thank Max Planck Institute for Astrophysics for computational support.

REFERENCES

Ahmad I., Greene J. P., Moore E. F., Ghelberg S., Ofan A., Paul M., Kutschera W., 2006, PhRvC, 74, 065803
Arnett D., 1996, Supernovae and Nucleosynthesis: An Investigation of the History of Matter from the Big Bang to the Present, Princeton Univ. Press, Princeton, NJ
Bamba A., Yamazaki R., Hiraga J. S., 2005, ApJ, 632, 294
Bietenholz M. F., Bartel N., 2008, MNRAS, 386, 1411
Bird, A. J., et al. 2006, ApJ, 636, 765
Boggs S. E., et al., 2015, Science, 348, 670
Borkowski K. J., Reynolds S. P., Green D. A., Hwang U., Petre R., Krishnamurthy K., Willett R., 2010, ApJ, 724, L161
Camilo F., Ransom S. M., Gaensler B. M., Slane P. O., Lorimer D. R., Reynolds J., Manchester R. N., Murray S. S., 2006, ApJ, 637, 456
Carlton A. K., Borkowski K. J., Reynolds S. P., Hwang U., Petre R., Green D. A., Krishnamurthy K., Willett R., 2011, ApJ, 737, L22
Caballero I., et al., 2013, proceedings of the 9th INTEGRAL Workshop, Eds. A. Goldwurm, F. Lebrun and C. Winkler, id 142, arXiv:1304.1349
Churazov E., Sunyaev R., Sazonov S., Revnivtsev M., Varshalovich D., 2005, MNRAS, 357, 1377
Churazov E., et al., 2007, A&A, 467, 529
Churazov, E., Sunyaev, R., Isern, J., et al. 2014, Nature, 512, 406
Dufour F., Kaspi V. M., 2013, ApJ, 775, 52
Dupraz C., Bloemen H., Bennett K., Diehl R., Hermsen W., Iyudin A. F., Ryan J., Schoenfelder V., 1997, A&A, 324, 683
Fink M., Röpke F. K., Hillebrandt W., Seitenzahl I. R., Sim S. A., Kromer M., 2010, A&A, 514, AA53
Gotthelf E. V., Vasisht G., Boylan-Kolchin M., Torii K., 2000, ApJ, 542, L37
Grebenev S. A., Lutovinov A. A., Tsygankov S. S., Winkler C., 2012, Nature, 490, 373
Green, D. A. 2014, Bulletin of the Astronomical Society of India, 42, 47
Grefenstette B. W., et al., 2014, Nature, 506, 339
Gros, A., Goldwurm, A., Cadolle-Bel, M., et al. 2003, A&A, 411, L179
Hayato A., et al., 2010, ApJ, 725, 894
Hiraga J. S., et al., 2009, PASJ, 61, 275
Iwamoto K., Brachwitz F., Nomoto K., Kishimoto N., Umeda H., Hix W. R., Thielemann F.-K., 1999, ApJS, 125, 439
Iyudin A. F., et al., 1994, A&A, 284, L1
Iyudin A. F., et al., 1999, ApL&C, 38, 383
Iyudin A. F., et al., 1998, Nature, 396, 142
Iyudin A. F., Aschenbach B., Becker W., Dennerl K., Haberl F., 2005, A&A, 429, 225
Katsuda S., Tsunemi H., Mori K., 2008, ApJ, 678, L35
Kothes R., 2013, A&A, 560, A18
Krause O., Birkmann S. M., Usuda T., Hattori T., Goto M., Rieke G. H., Misselt K. A., 2008a, Science, 320, 1195
Krause O., Tanaka M., Usuda T., Hattori T., Goto M., Birkmann S., Nomoto K., 2008b, Nature, 456, 617
Krivonos, R., Revnivtsev, M., Lutovinov, A., Sazonov, S., Churazov, E., & Sunyaev, R. 2007, A&A, 475, 775
Krivonos R., Revnivtsev M., Tsygankov S., Sazonov S., Vikhlinin A., Pavlinsky M., Churazov E., Sunyaev R., 2010a, A&A, 519, A107
Krivonos, R., Tsygankov, S., Revnivtsev, M., et al. 2010b, A&A, 523, A61
Krivonos, R., Tsygankov, S., Lutovinov, A., et al. 2012, A&A, 545, AA27
Leahy D. A., Tian W. W., 2008, A&A, 480, L25
Lebrun, F., Leray, J. P., Lavocat, P., et al. 2003, A&A, 411, L141
Liu, Q. Z., van Paradijs, J., & van den Heuvel, E. P. J. 2007, A&A, 469, 807
Lopez L. A., et al., 2015, ApJ, 814, 132
Maeda K., Röpke F. K., Fink M., Hillebrandt W., Travaglio C., Thielemann F.-K., 2010, ApJ, 712, 624
Magkotsios G., Timmes F. X., Hungerford A. L., Fryer C. L., Young P. A., Wiescher M., 2010, ApJS, 191, 66
Miceli M., Sciortino S., Troja E., Orlando S., 2015, ApJ, 805, 120
Nagataki S., Hashimoto M.-a., Sato K., Yamada S., Mochizuki Y. S., 1998, ApJ, 492, L45
Nomoto K., Thielemann F.-K., Yokoi K., 1984, ApJ, 286, 644
Reed J. E., Hester J. J., Fabian A. C., Winkler P. F., 1995, ApJ, 440, 706
Renaud M., Lebrun F., Ballet J., Decourchelle A., Terrier R., Prantzos N., 2004, ESASP, 552, 81
Renaud M., et al., 2006a, ApJ, 647, L41
Renaud M., Vink J., Decourchelle A., Lebrun F., Terrier R., Ballet J., 2006b, NewAR, 50, 540
Renaud M., et al., 2010, ApJ, 716, 663
Reynolds S. P., 1998, ApJ, 493, 375
Reynolds S. P., Borkowski K. J., Hwang U., Hughes J. P., Badenes C., Laming J. M., Blondin J. M., 2007, ApJ, 668, L135
Reynolds S. P., Borkowski K. J., Green D. A., Hwang U., Harrus I., Petre R., 2008, ApJ, 680, L41
Sankrit R., Blair W. P., Delaney T., Rudnick L., Harrus I. M., Ennis J. A., 2005, AdSpR, 35, 1027
Schönfelder V., et al., 2000, AIPC, 510, 54
Siegert T., Diehl R., Krause M. G. H., Greiner J., 2015, A&A, 579, A124
Slane P., Hughes J. P., Edgar R. J., Plucinsky P. P., Miyata E., Tsunemi H., Aschenbach B., 2001, ApJ, 548, 814
The L.-S., et al., 2006, A&A, 450, 1037
Thorstensen J. R., Fesen R. A., van den Bergh S., 2001, AJ, 122, 297
Timmes F. X., Woosley S. E., Hartmann D. H., Hoffman R. D., 1996, ApJ, 464, 332
Trimble V., 1973, PASP, 85, 579

Troja E., et al., 2014, ApJ, 797, LL6
Tsunemi H., Miyata E., Aschenbach B., Hiraga J., Akutsu D., 2000, PASJ, 52, 887
Ubertini, P., Lebrun, F., Di Cocco, G., et al. 2003, A&A, 411, L131
Vink J., Laming J. M., Kaastra J. S., Bleeker J. A. M., Bloemen H., Oberlack U., 2001, ApJ, 560, L79
Vink J., 2012, A&ARv, 20, 49
Wang W., Li Z., 2014, ApJ, 789, 123
Winkler C., et al., 2003, A&A, 411, L1
Winkler P. F., Gupta G., Long K. S., 2003, ApJ, 585, 324
Woosley S. E., Kasen D., 2011, ApJ, 734, 38
Zhang B., Zheng X. W., Reid M. J., Menten K. M., Xu Y., Moscadelli L., Brunthaler A., 2009, ApJ, 693, 419
Zirakashvili V. N., Aharonian F., 2007, A&A, 465, 695
Zoglauer A., et al., 2015, ApJ, 798, 98

Table 2. The complete catalogue of Galactic SNRs (Green, 2014) with measured fluxes or 3σ upper limits in the $64.6-82.2$ keV band. This catalogue is only available in the online version of the paper.

No.	Name[1]	l^{II} deg	b^{II} deg	Flux$_{64.6-82.2\ \mathrm{keV}}$[2] 10^{-12}erg cm^{-2} s^{-1}	Notes[3]
001	SNR G000.0+00.0	-0.042	-0.054	N/A	confusion (AX J1745.6-2901)
002	SNR G000.3+00.0	0.330	0.040	N/A	confusion (1E 1743.1-2843)
003	SNR G000.9+00.1	0.869	0.084	N/A	confusion (IGR J17464-2811)
004	SNR G001.0−00.1	1.000	-0.133	N/A	confusion (IGR J17475-2822)
					confusion (IGR J17497-2821, IGR J17464-2811)
005	SNR G001.4−00.1	1.460	-0.154	N/A	confusion (AX J1749.1-2733)
006	SNR G001.9+00.3	1.871	0.326	< 1.11	G1.9+0.3
007	SNR G003.7−00.2	3.781	-0.280	< 1.16	
008	SNR G003.8+00.3	3.810	0.395	< 1.16	
009	SNR G004.2−03.5	4.210	-3.506	< 1.22	
010	SNR G004.5+06.8	4.526	6.820	< 1.50	Kepler SN1604
011	SNR G004.8+06.2	4.798	6.243	< 1.46	
012	SNR G005.2−02.6	5.197	-2.600	< 1.23	
013	SNR G005.4−01.2	5.348	-1.133	N/A	confusion (GX 5-1)
014	SNR G005.5+00.3	5.551	0.322	< 1.23	
015	SNR G005.9+03.1	5.905	3.130	< 1.33	
016	SNR G006.1+00.5	6.104	0.532	< 1.26	
017	SNR G006.1+01.2	6.096	1.209	< 1.26	
018	SNR G006.4+04.0	6.416	4.026	< 1.40	
019	SNR G006.4−00.1	6.435	-0.076	< 1.26	
020	SNR G006.5−00.4	6.510	-0.478	< 1.26	
021	SNR G007.0−00.1	7.050	-0.078	< 1.29	
022	SNR G007.2+00.2	7.200	0.197	< 1.30	
023	SNR G007.7−03.7	7.754	-3.771	< 1.40	
024	SNR G008.3−00.0	8.304	-0.095	< 1.38	
025	SNR G008.7−00.1	8.744	-0.096	< 1.41	
026	SNR G008.7−05.0	8.712	-5.011	< 1.56	
027	SNR G008.9+00.4	8.903	0.403	< 1.42	
028	SNR G009.7−00.0	9.699	-0.062	< 1.71	confusion (SGR 1806-20)
029	SNR G009.8+00.6	9.749	0.566	< 1.52	
030	SNR G009.9−00.8	9.958	-0.805	< 1.52	
031	SNR G010.5−00.0	10.599	-0.036	< 1.56	
032	SNR G011.0−00.0	11.027	-0.051	< 1.78	confusion (XTE J1810-189)
033	SNR G011.1+00.1	11.184	0.112	< 1.78	confusion (XTE J1810-189)
034	SNR G011.1−00.7	11.143	-0.713	< 1.78	confusion (PSR J1811-1925)
035	SNR G011.1−01.0	11.171	-1.042	< 1.64	G11.2-0.3 SN386
036	SNR G011.2−00.3	11.184	-0.337	< 1.78	continuum (PSR J1811-1925)
037	SNR G011.4−00.1	11.400	-0.038	< 1.78	confusion (XTE J1810-189)
038	SNR G011.8−00.2	11.893	-0.208	< 1.67	confusion (SNR G012.0−00.1)
039	SNR G012.0−00.1	11.969	-0.104	< 1.67	confusion (SNR G011.8−00.2)
040	SNR G012.2+00.3	12.260	0.300	< 1.69	
041	SNR G012.5+00.2	12.588	0.222	< 1.91	confusion (IGR J18135-1751)
042	SNR G012.7−00.0	12.727	0.004	< 1.91	confusion (IGR J18135-1751)
043	SNR G012.8−00.0	12.834	-0.019	< 1.91	confusion (IGR J18135-1751)
044	SNR G013.3−01.3	13.319	-1.302	< 1.75	
045	SNR G013.5+00.2	13.446	0.147	< 1.86	confusion (GX 13+1)
046	SNR G014.1−00.1	14.177	-0.118	< 1.91	confusion (SNR G014.3+00.1)
047	SNR G014.3+00.1	14.303	0.141	< 1.91	confusion (SNR G014.1−00.1)
048	SNR G015.1−01.6	15.109	-1.612	< 1.88	
049	SNR G015.4+00.1	15.419	0.179	< 1.86	confusion (IGR J18175-1530)
050	SNR G015.9+00.2	15.881	0.199	< 1.88	
051	SNR G016.0−00.5	16.054	-0.548	< 1.91	
052	SNR G016.2−02.7	16.125	-2.614	< 1.95	
053	SNR G016.4−00.5	16.412	-0.549	< 1.92	
054	SNR G016.7+00.1	16.734	0.089	< 1.89	confusion (AX J1820.5-1434)
055	SNR G017.0−00.0	17.026	-0.035	< 1.89	confusion (SNR G016.7+00.1, IGR J18219-1347)

Continued on next page

Table 2 – continued from previous page

No.	Name[1]	l^{II} deg	b^{II} deg	$\mathrm{Flux}_{64.6-82.2\ \mathrm{keV}}$[2] 10^{-12}erg cm^{-2} s^{-1}	Notes[3]
056	SNR G017.4−00.1	17.485	-0.116	< 1.89	confusion (IGR J18219-1347)
057	SNR G017.4−02.3	17.388	-2.297	< 2.00	
058	SNR G017.8−02.6	17.795	-2.608	< 2.03	
059	SNR G018.1−00.1	18.163	-0.151	< 2.03	
060	SNR G018.6−00.2	18.627	-0.278	< 1.95	
061	SNR G018.8+00.3	18.802	0.353	< 1.95	
062	SNR G018.9−01.1	18.952	-1.185	< 2.04	
063	SNR G019.1+00.2	19.148	0.269	< 1.95	
064	SNR G020.0−00.2	19.983	-0.171	< 1.98	
065	SNR G020.4+00.1	20.469	0.158	< 1.98	
066	SNR G021.0−00.4	21.043	-0.470	< 2.00	
067	SNR G021.5−00.1	21.562	-0.097	< 2.00	confusion (AX J183039-1002)
068	SNR G021.5−00.9	21.487	-0.890	7.8 ± 0.67 (11.64)	continuum SNR 021.5-00.9; $F_{78} < 9 \times 10^{-6}$ ph cm^{-2} s^{-1}
069	SNR G021.6−00.8	21.648	-0.839	< 2.01	confusion (SNR 021.5-00.9)
070	SNR G021.8−00.6	21.795	-0.508	< 2.11	
071	SNR G022.7−00.2	22.665	-0.194	< 2.01	
072	SNR G023.3−00.3	23.206	-0.331	< 2.03	
073	SNR G023.6+00.3	23.530	0.311	< 0.52	confusion (IGR J18325-0756)
074	SNR G024.7+00.6	24.663	0.588	< 2.04	
075	SNR G024.7−00.6	24.782	-0.621	< 2.07	
076	SNR G025.1−02.3	25.097	-2.255	< 2.15	
077	SNR G027.4+00.0	27.389	-0.004	2.94 ± 0.67 (4.39)	continuum (IGR J18325-0756); $F_{78} < 1 \times 10^{-5}$ ph cm^{-2} s^{-1}
078	SNR G027.8+00.6	27.694	0.569	< 2.08	
079	SNR G028.6−00.1	28.619	-0.100	< 2.10	
080	SNR G028.8+01.5	28.917	1.433	< 2.10	
081	SNR G029.6+00.1	29.558	0.115	< 2.22	
082	SNR G029.7−00.3	29.705	-0.244	4.80 ± 0.69 (6.96)	continuum (PSR J1846-0258); $F_{78} < 1 \times 10^{-5}$ ph cm^{-2} s^{-1}
083	SNR G030.7+01.0	30.719	0.955	< 2.08	
084	SNR G030.7−02.0	30.689	-1.984	< 2.28	
085	SNR G031.5−00.6	31.551	-0.631	< 2.07	
086	SNR G031.9+00.0	31.886	0.032	< 2.28	confusion (IGR J18486-0047)
087	SNR G032.0−04.9	31.916	-4.606	< 2.28	
088	SNR G032.1−00.9	32.120	-0.901	< 2.17	confusion (IGR J18538-0102)
089	SNR G032.4+00.1	32.407	0.111	< 2.17	
090	SNR G032.8−00.1	32.811	-0.056	< 2.03	
091	SNR G033.2−00.6	33.175	-0.548	< 2.01	
092	SNR G033.6+00.1	33.695	0.009	< 2.00	
093	SNR G034.7−00.4	34.668	-0.392	< 1.97	
094	SNR G035.6−00.4	35.643	-0.430	< 1.92	
095	SNR G036.6+02.6	36.582	2.602	< 1.95	
096	SNR G036.6−00.7	36.585	-0.695	< 1.89	
097	SNR G038.7−01.3	38.644	-1.341	< 1.83	
098	SNR G039.2−00.3	39.243	-0.321	< 1.81	
099	SNR G039.7−02.0	39.694	-2.387	< 1.91	confusion (SS 433)
100	SNR G040.5−00.5	40.522	-0.509	< 1.83	
101	SNR G041.1−00.3	41.115	-0.314	< 1.81	
102	SNR G041.5+00.4	41.480	0.359	< 1.83	
103	SNR G042.0−00.1	41.953	-0.047	< 1.81	
104	SNR G042.8+00.6	42.820	0.635	< 1.91	confusion (SGR 1900+14)
105	SNR G043.3−00.2	43.267	-0.190	< 1.91	confusion (IGR J19108+0917)
106	SNR G043.9+01.6	43.908	1.614	< 1.89	
107	SNR G045.7−00.4	45.686	-0.390	< 2.06	confusion (GRS 1915+105)
108	SNR G046.8−00.3	46.771	-0.302	< 1.94	
109	SNR G049.2−00.7	49.140	-0.603	< 2.08	
110	SNR G053.6−02.2	53.626	-2.261	< 2.59	
111	SNR G054.1+00.3	54.094	0.260	< 2.64	
112	SNR G054.4−00.3	54.474	-0.291	< 2.67	
113	SNR G055.0+00.3	55.110	0.419	< 2.79	

Continued on next page

Table 2 – continued from previous page

No.	Name[1]	l[11] deg	b[11] deg	Flux$_{64.6-82.2\ \mathrm{keV}}$[2] 10^{-12}erg cm^{-2} s^{-1}	Notes[3]
114	SNR G055.7+03.4	55.599	3.515	< 3.03	
115	SNR G057.2+00.8	57.300	0.833	< 2.97	
116	SNR G059.5+00.1	59.579	0.116	< 3.03	
117	SNR G059.8+01.2	59.807	1.200	< 3.03	
118	SNR G063.7+01.1	63.786	1.165	< 2.82	
119	SNR G064.5+00.9	64.517	0.942	< 2.76	
120	SNR G065.1+00.6	65.268	0.302	< 2.71	
121	SNR G065.3+05.7	65.179	5.661	< 2.98	
122	SNR G065.7+01.2	65.716	1.208	1.92 ± 0.89 (2.16)	
123	SNR G065.8−00.5	65.844	-0.546	< 2.71	
124	SNR G066.0−00.0	66.027	-0.048	< 2.67	
125	SNR G067.6+00.9	67.581	0.924	< 2.55	
126	SNR G067.7+01.8	67.738	1.823	< 2.55	
127	SNR G067.8+00.5	67.806	0.495	< 2.55	
128	SNR G068.6−01.2	68.603	-1.204	< 2.56	
129	SNR G069.0+02.7	68.837	2.778	2.02 ± 0.84 (2.41)	
130	SNR G069.7+01.0	69.690	1.000	< 2.43	
131	SNR G073.9+00.9	73.912	0.883	< 2.25	
132	SNR G074.0−08.5	73.982	-8.564	< 3.36	
133	SNR G074.9+01.2	74.942	1.141	< 2.28	confusion (IGR J20159+3713)
134	SNR G076.9+01.0	76.895	0.972	< 2.19	
135	SNR G078.2+02.1	78.143	2.186	< 2.21	
136	SNR G082.2+05.3	82.150	5.316	< 2.56	
137	SNR G083.0−00.3	83.002	-0.272	< 2.28	
138	SNR G084.2−00.8	84.195	-0.807	< 2.33	
139	SNR G085.4+00.7	85.366	0.783	< 2.37	
140	SNR G085.9−00.6	85.906	-0.607	< 2.38	
141	SNR G089.0+04.7	88.838	4.794	< 2.73	
142	SNR G093.3+06.9	93.278	6.906	< 3.17	
143	SNR G093.7−00.2	93.754	-0.218	< 2.62	
144	SNR G094.0+01.0	93.974	1.026	< 2.64	
145	SNR G096.0+02.0	96.043	1.953	< 2.79	
146	SNR G106.3+02.7	106.273	2.705	< 2.54	
147	SNR G108.2−00.6	108.193	-0.627	< 2.27	
148	SNR G109.1−01.0	109.142	-1.015	2.63 ± 0.73 (3.60)	continuum (2E 2259.0+5836); $F_{78} < 1 \times 10^{-5}$ ph cm^{-2} s^{-1}
149	SNR G111.7−02.1	111.734	-2.145	7.31 ± 0.68 (10.75)	Cas A
150	SNR G113.0+00.2	114.088	-0.213	< 1.89	
151	SNR G114.3+00.3	114.292	0.300	< 1.88	
152	SNR G116.5+01.1	116.485	1.104	< 1.84	
153	SNR G116.9+00.2	116.926	0.173	< 1.84	
154	SNR G119.5+10.2	119.579	10.170	< 3.18	
155	SNR G120.1+01.4	120.087	1.423	2.20 ± 0.63 (3.50)	continuum (Tycho SNR); $F_{78} < 9 \times 10^{-6}$ ph cm^{-2} s^{-1}
156	SNR G126.2+01.6	126.245	1.575	< 2.27	
157	SNR G127.1+00.5	127.081	0.593	< 2.34	
158	SNR G130.7+03.1	130.728	3.075	< 2.94	
159	SNR G132.7+01.3	132.621	1.512	< 3.13	
160	SNR G152.4−02.1	152.560	-2.052	< 3.41	
161	SNR G156.2+05.7	156.115	5.663	< 3.78	
162	SNR G159.6+07.3	159.598	7.300	< 4.20	
163	SNR G160.9+02.6	160.436	2.787	< 3.70	
164	SNR G166.0+04.3	166.116	4.278	< 4.75	
165	SNR G178.2−04.2	179.411	-2.361	< 3.22	
166	SNR G179.0+02.6	179.052	2.597	< 4.00	
167	SNR G180.0−01.7	-179.830	-1.819	< 3.18	
168	SNR G182.4+04.3	-177.583	4.299	< 3.99	
169	SNR G184.6−05.8	-175.446	-5.786	N/A	continuum (Crab Nebula)
170	SNR G189.1+03.0	-170.967	2.978	< 3.70	
171	SNR G190.9−02.2	-169.027	-2.128	< 3.27	

Continued on next page

Table 2 – continued from previous page

No.	Name[1]	l^{II} deg	b^{II} deg	$\mathrm{Flux}_{64.6-82.2\ \mathrm{keV}}$[2] 10^{-12}erg cm^{-2} s^{-1}	Notes[3]
172	SNR G192.8−01.1	-167.234	-1.109	< 3.62	
173	SNR G205.5+00.5	-154.268	0.209	< 6.60	
174	SNR G206.9+02.3	-153.112	2.315	< 7.06	
175	SNR G213.0−00.6	-146.692	-0.363	< 5.49	
176	SNR G260.4−03.4	-99.600	-3.439	< 2.22	
177	SNR G261.9+05.5	-98.052	5.478	< 2.75	confusion (1RXS J090431.1-382920)
178	SNR G263.9−03.3	-96.061	-3.368	< 2.07	
179	SNR G266.2−01.2	-93.741	-1.220	< 2.04	Vela Jr
180	SNR G272.2−03.2	-87.783	-3.181	< 2.46	
181	SNR G279.0+01.1	-81.368	1.219	< 3.01	
182	SNR G284.3−01.8	-75.691	-1.783	< 2.69	
183	SNR G286.5−01.2	-73.434	-1.214	< 2.56	
184	SNR G289.7−00.3	-70.315	-0.293	< 2.49	
185	SNR G290.1−00.8	-69.851	-0.780	< 2.50	
186	SNR G291.0−00.1	-68.977	-0.084	< 2.49	
187	SNR G292.0+01.8	-67.970	1.755	< 2.49	
188	SNR G292.2−00.5	-67.837	-0.536	< 2.61	
189	SNR G293.8+00.6	-66.230	0.605	< 2.50	
190	SNR G294.1−00.0	-65.884	-0.057	< 2.52	
191	SNR G296.1−00.5	-63.947	-0.503	< 2.55	
192	SNR G296.5+10.0	-63.512	9.932	< 3.57	
193	SNR G296.7−00.9	-63.339	-0.945	< 2.58	
194	SNR G296.8−00.3	-63.119	-0.335	< 2.56	
195	SNR G298.5−00.3	-61.472	-0.327	< 2.54	
196	SNR G298.6−00.0	-61.394	-0.062	< 2.54	
197	SNR G299.2−02.9	-60.815	-2.892	< 2.67	
198	SNR G299.6−00.5	-60.413	-0.471	< 2.54	
199	SNR G301.4−01.0	-58.559	-0.984	< 2.50	
200	SNR G302.3+00.7	-57.713	0.731	< 2.46	
201	SNR G304.6+00.1	-55.401	0.125	< 2.42	
202	SNR G306.3−00.9	-53.693	-0.894	< 2.42	
203	SNR G308.1−00.7	-51.867	-0.662	< 2.42	
204	SNR G308.4−01.4	-28.346	-23.068	< 5.80	
205	SNR G308.8−00.1	-51.189	-0.096	< 2.42	
206	SNR G309.2−00.6	-50.843	-0.696	< 2.43	
207	SNR G309.8+00.0	-50.215	0.000	< 2.44	
208	SNR G310.6−00.3	-49.380	-0.276	< 2.46	
209	SNR G310.6−01.6	-49.410	-1.597	3.51 ± 0.83 (4.23)	continuum (IGR J14003-6326); $F_{78} < 1 \times 10^{-5}$ ph cm^{-2} s^{-1}
210	SNR G310.8−00.4	-49.189	-0.465	< 2.47	
211	SNR G311.5−00.3	-48.469	-0.340	< 2.49	
212	SNR G312.4−00.4	-47.571	-0.375	< 2.52	
213	SNR G312.5−03.0	-47.512	-3.003	< 2.59	
214	SNR G315.1+02.7	-44.914	2.826	2.26 ± 0.89 (2.53)	
215	SNR G315.4−00.3	-44.587	-0.285	< 2.62	
216	SNR G315.4−02.3	-44.583	-2.364	< 2.69	
217	SNR G315.9−00.0	-44.138	-0.025	< 2.64	
218	SNR G316.3−00.0	-43.712	-0.013	< 2.66	
219	SNR G317.3−00.2	-42.686	-0.238	< 2.67	
220	SNR G318.2+00.1	-41.785	0.094	< 2.69	
221	SNR G318.9+00.4	-41.094	0.391	< 2.70	
222	SNR G320.4−01.2	-39.615	-1.198	27.04 ± 0.91 (29.71)	continuum (PSR 1509-58); $F_{78} < 1 \times 10^{-5}$ ph cm^{-2} s^{-1}
223	SNR G320.6−01.6	-39.322	-1.536	< 2.75	
224	SNR G321.9−00.3	-38.099	-0.298	< 2.79	
225	SNR G321.9−01.1	-38.109	-1.066	< 2.69	
226	SNR G322.1+00.0	-37.866	0.028	< 2.79	confusion (4U 1516-569)
227	SNR G322.5−00.1	-37.537	-0.106	< 2.79	
228	SNR G323.5+00.1	-36.514	0.112	< 2.58	
229	SNR G326.3−01.8	-33.705	-1.763	< 2.58	

Continued on next page

Table 2 – continued from previous page

No.	Name[1]	l[II] deg	b[II] deg	Flux$_{64.6-82.2\ \mathrm{keV}}$[2] 10^{-12}erg cm^{-2} s^{-1}	Notes[3]
230	SNR G327.1−01.1	-32.904	-1.106	< 2.38	
231	SNR G327.2−00.1	-32.757	-0.128	7.20 ± 0.78 (9.23)	continuum (1E 1547.0-5408); $F_{78} < 1 \times 10^{-5}$ ph cm^{-2} s^{-1}
232	SNR G327.4+00.4	-32.752	0.486	< 2.34	
233	SNR G327.4+01.0	-32.631	1.007	< 2.33	
234	SNR G327.6+14.6	-32.428	14.566	< 3.00	SN 1006
235	SNR G328.4+00.2	-31.589	0.229	< 2.27	
236	SNR G329.7+00.4	-30.280	0.406	< 2.16	
237	SNR G330.0+15.0	-30.199	15.534	< 3.01	
238	SNR G330.2+01.0	-29.827	0.983	< 2.13	
239	SNR G332.0+00.2	-27.954	0.210	< 2.03	
240	SNR G332.4+00.1	-27.593	0.120	< 2.00	
241	SNR G332.4−00.4	-27.572	-0.363	< 2.00	confusion (IGR J16175-5059)
242	SNR G332.5−05.6	-27.421	-5.575	< 2.27	
243	SNR G335.2+00.1	-24.819	0.060	< 2.00	confusion (IGR J16283-4838)
244	SNR G336.7+00.5	-23.245	0.531	< 1.95	confusion (4U 1630-47)
245	SNR G337.0−00.1	-23.022	-0.129	< 1.95	confusion (IGR J16358-4726)
246	SNR G337.2+00.1	-22.828	0.055	< 1.95	confusion (4U 1630-47, IGR J16358-4726)
247	SNR G337.2−00.7	-22.811	-0.736	< 1.86	
248	SNR G337.3+01.0	-22.667	0.962	< 1.88	
249	SNR G337.8−00.1	-22.215	-0.102	< 1.95	confusion (AX J163904-4642)
250	SNR G338.1+00.4	-21.900	0.420	< 1.95	confusion (AX J163904-4642)
251	SNR G338.3−00.0	-21.678	-0.079	< 1.95	confusion (AX J163904-4642)
252	SNR G338.5+00.1	-21.474	0.067	< 1.83	
253	SNR G340.4+00.4	-19.598	0.448	< 1.80	confusion (SNR G340.6+00.3)
254	SNR G340.6+00.3	-19.401	0.344	< 1.80	confusion (SNR G340.4+00.4)
255	SNR G341.2+00.9	-18.814	0.864	< 1.94	confusion (IGR J16493-4348)
256	SNR G341.9−00.3	-18.140	-0.317	< 1.78	confusion (SNR G342.0−00.2)
257	SNR G342.0−00.2	-18.057	-0.207	< 1.78	confusion (SNR G341.9−00.3)
258	SNR G342.1+00.9	-17.899	0.888	< 1.78	
259	SNR G343.0−06.0	-17.012	-6.035	< 2.07	
260	SNR G343.1−00.7	-16.919	-0.594	< 1.92	confusion (IGR J17014-4306)
261	SNR G343.1−02.3	-16.909	-2.310	< 1.94	confusion (4U 1705-440)
262	SNR G344.7−00.1	-15.319	-0.156	< 1.71	
263	SNR G345.7−00.2	-14.273	-0.184	< 1.67	
264	SNR G346.6−00.2	-13.373	-0.221	< 1.74	confusion (1RXS J170849.0-400910)
265	SNR G347.3−00.5	-12.626	-0.509	< 1.69	
266	SNR G348.5+00.1	-11.609	0.161	< 1.69	
267	SNR G348.5−00.0	-11.403	-0.012	< 1.69	
268	SNR G348.7+00.3	-11.346	0.395	< 1.52	
269	SNR G349.2−00.1	-10.870	-0.070	< 1.52	confusion (IGR J17164-3803)
270	SNR G349.7+00.2	-10.269	0.177	< 1.46	confusion (SNR G350.1−00.3)
271	SNR G350.0−02.0	-10.078	-2.046	< 1.47	
272	SNR G350.1−00.3	-10.278	0.248	< 1.46	confusion (SNR G349.7+00.2)
273	SNR G351.2+00.1	-8.732	0.158	< 1.36	
274	SNR G351.7+00.8	-8.296	0.817	< 1.42	
275	SNR G351.9−00.9	-8.077	-0.960	< 1.33	
276	SNR G352.7−00.1	-7.255	-0.120	< 1.29	
277	SNR G353.6−00.7	-6.445	-0.649	< 1.27	
278	SNR G353.9−02.0	-6.059	-2.085	< 1.27	
279	SNR G354.1+00.1	-5.811	0.146	< 1.32	confusion (GX 354-0)
280	SNR G354.8−00.8	-5.128	-0.783	< 1.22	
281	SNR G355.4+00.7	-4.597	0.727	< 1.27	confusion (IGR J17315-3221)
282	SNR G355.6−00.0	-4.313	-0.078	< 1.27	confusion (IGR J17353-3257)
283	SNR G355.9−02.5	-4.054	-2.535	< 1.20	
284	SNR G356.2+04.5	-3.782	4.464	< 1.29	
285	SNR G356.3−00.3	-3.701	-0.355	< 1.16	
286	SNR G356.3−01.5	-3.690	-1.503	0.86 ± 0.39 (2.22)	
287	SNR G357.7+00.3	-2.332	0.348	< 1.22	

Continued on next page

Table 2 – continued from previous page

No.	Name[1]	l^{II} deg	b^{II} deg	$Flux_{64.6-82.2\ keV}$[2] 10^{-12}erg cm^{-2} s^{-1}	Notes[3]
288	SNR G357.7−00.1	-2.312	-0.121	< 1.12	
289	SNR G358.0+03.8	-2.035	3.803	< 1.22	
290	SNR G358.1+00.1	-1.881	1.038	< 1.12	
291	SNR G358.5−00.9	-1.416	-1.002	< 1.11	
292	SNR G359.0−00.9	-0.999	-0.917	< 1.11	confusion (SLX1744-299/300)
293	SNR G359.1+00.9	-0.903	0.988	< 1.17	
294	SNR G359.1−00.5	-0.879	-0.506	< 1.17	confusion (IGR J17446-2947)

[1] Catalogue is sorted by source name, which is in turn, based on Galactic coordinates.
[2] The upper limits are given at 3σ confidence level. In case of a source detection, the significance is shown in parenthesis.
[3] The spatial confusion with a known hard X-ray source (shown in parenthesis) is indicated. SNRs dominated by the continuum flux are marked as well. If significance of the detection of such source is above 3σ level, an upper limit (3σ) in the 78.4 keV line is shown assuming a simple power-law continuum model.